HHS Public Access

Author manuscript

Clin Cancer Res. Author manuscript; available in PMC 2019 October 01.

Published in final edited form as:

Clin Cancer Res. 2018 October 01; 24(19): 4798–4807. doi:10.1158/1078-0432.CCR-17-3284.

Parallel Accumulation of Tumor Hyaluronan, Collagen, and Other Drivers of Tumor Progression

Xiaoming Li[1], **Michael H. Shepard**[1], **Jessica A. Cowell**[1], **Chunmei Zhao**[1], **Ryan J. Osgood**[1], **Sanna Rosengren**[1], **Barbara Blouw**[1], **Sheryl A. Garrovillo**[1], **Mark D. Pagel**[2], **Clifford J. Whatcott**[3], **Haiyong Han**[3], **Daniel D. Von Hoff**[3], **Darin M. Taverna**[1], **Michael J. LaBarre**[1], **Daniel C. Maneval**[1], **Curtis B. Thompson**[1]

[1]Halozyme Therapeutics, Inc., San Diego, California.

[2]Department of Cancer Systems Imaging, University of Texas, MD Anderson Cancer Center, Houston, Texas.

[3]Clinical Translational Research Division, Translational Genomics Research Institute (TGen), Phoenix, Arizona.

Abstract

Purpose: The tumor microenvironment (TME) evolves to support tumor progression. One marker of more aggressive malignancy is hyaluronan (HA) accumulation. Here, we characterize biological and physical changes associated with HA-accumulating (HA-high) tumors.

Experimental Design: We used immunohistochemistry, *in vivo* imaging of tumor pH, and microdialysis to characterize the TME of HA-high tumors, including tumor vascular structure, hypoxia, tumor perfusion by doxorubicin, pH, content of collagen. and smooth muscle actin (α-SMA). A novel method was developed to measure real-time tumor-associated soluble cytokines and growth factors. We also evaluated biopsies of murine and pancreatic cancer patients to investigate HA and collagen content, important contributors to drug resistance.

Corresponding Author: Curtis B. Thompson, Halozyme Therapeutics, Inc., 11388 Sorrento Valley Road, San Diego, CA 92121. Phone: 858-704-8166; Fax: 858-704-8301, cthompson@halozyme.com.

Authors' Contributions

Conception and design: H.M. Shepard, J.A. Cowell, R.J. Osgood, D.D. Von Hoff, D.C. Maneval, C.B. Thompson

Development of methodology: X. Li, J.A. Cowell, C. Zhao, R.J. Osgood, B. Blouw

Acquisition of data (provided animals, acquired and managed patients, provided facilities, etc.): J.A. Cowell, C. Zhao, R.J. Osgood, S. Rosengren, S.A. Garrovillo, M.D. Pagel, C.J. Whatcott, H. Han, D.D. Von Hoff

Analysis and interpretation of data (e.g., statistical analysis, biostatistics, computational analysis): X. Li, J.A. Cowell, R.J. Osgood, S. Rosengren, M.D. Pagel, C.J. Whatcott, H. Han, D.M. Taverna, C.B. Thompson

Writing, review, and/or revision of the manuscript: H.M. Shepard, J.A. Cowell, C. Zhao, R.J. Osgood, S. Rosengren, H. Han, D.D. Von Hoff, D.M. Taverna, M.J. LaBarre, D.C. Maneval, C.B. Thompson

Administrative, technical, or material support (i.e., reporting or organizing data, constructing databases): J.A. Cowell, R.J. Osgood

Study supervision: M.J. LaBarre, C.B. Thompson

Disclosure of Potential Conflicts of Interest

H.M. Shepard holds ownership interest (including patents) in and is a consultant/advisory board member for Halozyme Therapeutic, Inc. D.C. Maneval holds ownership interest (including patents) in Halozyme Therapeutic, Inc. No potential conflicts of interest were disclosed by the other authors.

Note: Supplementary data for this article are available at Clinical Cancer Research Online (http://clincancerres.aacrjournals.org/).

Results: In immunodeficient and immunocompetent mice, increasing tumor HA content is accompanied by increasing collagen content, vascular collapse, hypoxia, and increased metastatic potential, as reflected by increased α-SMA. *In vivo* treatment of HA-high tumors with PEGylated recombinant human hyaluronidase (PEGPH20) dramatically reversed these changes and depleted stores of VEGF-A165, suggesting that PEGPH20 may also diminish the angiogenic potential of the TME. Finally, we observed in xenografts and in pancreatic cancer patients a coordinated increase in HA and collagen tumor content.

Conclusions: The accumulation of HA in tumors is associated with high tIP, vascular collapse, hypoxia, and drug resistance. These findings may partially explain why more aggressive malignancy is observed in the HA-high phenotype. We have shown that degradation of HA by PEGPH20 partially reverses this phenotype and leads to depletion of tumor-associated VEGF-A165. These results encourage further clinical investigation of PEGPH20.

Introduction

Accumulation of hyaluronan (HA) is common in many cancers, and pancreatic cancer is one of the most common diseases giving rise to the HA-high phenotype (1). Accumulation of HA in pancreatic cancer predicts a less favorable outcome, as compared with tumors that have lower amounts of HA (2, 3). The glycosaminoglycan, HA, is an important component of the extracellular matrix, along with collagens, proteoglycans (e.g., versican, tenascin C), and other glycosaminoglycans (e.g., heparan sulfates, chondroitin sulfates; ref. 4). These molecules often have ionic charges that allow growth factors and cytokines to bind to them, accumulating a reserve to support ongoing tumor growth (5, 6). Collagen, other proteoglycans, and glycosaminoglycans are hygroscopic, and as they are synthesized within the tumor, they imbibe water molecules and expand, resulting in a dense mass of cellular and highly hydrated noncellular components (7). Elevated tumor interstitial pressure (tIP), as described in Thompson and colleagues (8) and Provenzano and colleagues (9), is associated with vascular collapse and the hypoxic phenotype (7, 10, 11). Mechanisms of hypoxia-associated tumor aggressiveness include upregulation of hypoxia-inducible factors, subsequent expression of proangiogenic proteins, and enhancement of the epithelial-to-mesenchymal transition (increased cellular migration). Hypoxia leads to generation of superoxides that can promote further mutagenesis, creation of a more aggressive tumor microenvironment (TME), tumor progression, and metastasis (11–17).

Therapeutic approaches that attempt to normalize the properties of hypoxic tumor growth will be valuable resources to add to the anticancer armamentarium. Experimental therapies have focused on increasing perfusion of hypoxic tumors (18). These efforts include targeting the cellular and noncellular components that lead to increased fluid and solid tIPs and drug resistance. Among the varied approaches have been depletion of stromal fibroblasts via inhibition of the hedgehog pathway (19); treatment with losartan, which inhibits stromal collagen synthesis (20); treatment with calcipotriol, which partially reverses the inflammatory stromal reaction, also leading to increased drug delivery to tumors (21); and treatment with compounds with antifibrotic properties which increase drug delivery, some of which are associated with reduced tumor HA and collagen (22, 23). HA accumulation occurs in subsets of many tumor types (1), where it contributes to vascular collapse and poor

perfusion often in combination with collagen (1, 8–10, 24). Clinical studies have shown a correlation of more aggressive disease with HA accumulation in tumors (2, 25). High tIP can be downmodulated through reduction of HA by the systemic administration of PEGylated recombinant human PH20 hyaluronidase (PEGPH20) or other forms of PH20 hyaluronidase (8, 9, 26–29), or by inhibition of HA synthesis (30, 31).

In this article, we describe the multifactorial but associated effects of hyaluronan accumulation and its depletion on the TME. This includes the parallel accumulation of collagen and HA, an observation that has been made in the context of wound repair (32). We also show that PEGPH20-mediated HA degradation leads to coordinated changes in the TME that result in less hypoxia, increased pH, and a TME that is depleted of its stores of VEGF-A165.

Materials and Methods

Cell culture and establishment of HA-accumulating tumor cell lines

BxPC-3 and AsPC-1, human pancreatic cancer cell lines, A549 and H2170 human non–small cell lung cancer cell lines, KLN205, a murine lung cancer cell line, and CT26, a murine colon cancer cell line, were purchased from the ATCC and authenticated by the ATCC (STR DNA profiling). WT-CLS1, a human Wilms' tumor cell line, was obtained from CLS Cell Lines Service and authenticated by CLS Cell Lines Service (STR DNA profiling). All cell lines were maintained in complete RPMI or DMEM supplemented with 10% FBS. To generate HA-accumulating cell lines, human hyaluronan synthase 3 (HAS3) cDNA (ID: IOH43733) was subcloned into a pLV-EF1a lentiviral vector (Biosettia), and A549, AsPC-1, BxPC-3, CT26, H2170, and WT-CLS1 parental cells were transduced with the resulting lentivirus pLV-EF1a-hHAS3-Hyg vector. Transfected cells were selected with hygromycin, and HA production was confirmed using a Hyaluronan DuoSet ELISA Kit (R&D Systems). Accumulation of HA was also determined by visualization of HA pericellular matrices via a particle-exclusion assay (8). All parental and engineered cell lines were routinely tested for Mycoplasma infection using the MycoAlert Mycoplasma Detection Kit and PCR (IDEXX). Only low-passage cell lines were used for study.

Establishment of parental and HA-accumulating xenograft and murine tumor models

Male athymic nu/nu, Balb/C, and DBA/2 mice, 5–6 weeks of age, were purchased from Taconic and handled in accordance with approved Institutional Animal Care and Use Committee protocols. Following acclimation, mice were inoculated with A549/HAS3, AsPC-1, AsPC-1/HAS3, BxPC-3, BxPC-3/HAS3, H2170/HAS3, WT-CLS1/HAS3 (5×10^6, athymic nu/nu), or CT26/HAS3 cells (2×10^5, Balb/C) adjacent to the right tibia periosteum. KLN205 cells were inoculated s.c. into the right flank of DBA/2 mice (31, 33). Tumor growth in peritibial models was determined by acquiring three-dimensional (3D) tumor images twice weekly using a high-resolution ultrasound imaging system (Vevo 2100; FUJIFILM VisualSonics), and subsequently the associated 3D tumor volume software was used to determine tumor volume. Subcutaneous tumors were measured using an electronic caliper (Vernier Software & Technology) and tumor volume in mm^3 calculated using the formula: Tumor volume = $1/2[\text{length} \times (\text{width})^2]$.

PEGylated recombinant human PH20 hyaluronidase (PEGPH20)

PEGPH20, provided by the Halozyme Therapeutics, Inc. formulation group, was generated by conjugating the N-hydroxysuccinimidyl ester of methoxypoly(ethylene glycol)-butanoic acid (MBA30K or PEG) to recombinant human hyaluronidase (rHuPH20) as previously described (8). The PEGylated rHuPH20 enzyme, PEGPH20, retained ≥25% of the initial specific activity of rHuPH20 (PEGPH20 at ~30,000 units/mg) and <0.05 endotoxin unit/mg protein and <1 ng DNA/mg protein. The PEGPH20 used in this study is the same as used in clinical trials.

Treatment schedule

When tumors reached ~1,500 mm^3, mice were staged into two groups: vehicle control and low-dose PEGPH20 (0.0375 mg/kg, i.v.); or three groups: vehicle control, low-dose PEGPH20, and high-dose PEGPH20 (1 mg/kg, i.v.), if a high-dose group was included. Unless indicated otherwise, test articles were administered on study day 1 and day 4 (q3dx2), and mice were euthanized 6 hours after the second dose. In pilot studies, this dosing paradigm was shown to reduce tumor HA by >80% in the high-dose (1 mg/kg) PEGPH20 groups (34).

Immunohistochemistry

Formalin-fixed, paraffin-embedded tumor sections were processed by standard methods for hematoxylin and eosin staining, immunohistochemistry (IHC), and immunofluorescence. HA staining was detected using a modified TNF-stimulated gene 6 protein (TSG-6, 0.25 μg/mL; Halozyme; ref. 35), followed by either fluorescein-HRP (Vector Labs) and Texas Red (Dako) staining or staining with the Intense R detection kit (Leica Biosystems). Collagen I (ColI) and α-SMA were detected using anti-ColI and anti–α-SMA antibodies, respectively (Abcam), followed by fluorescein-horseradish peroxidase (HRP) and fluorescein isothiocyanate (FITC; Dako) or DAB (Agilent). HA, ColI, and α-SMA were then imaged and quantified as described below.

Quantitative assessment of tumor perfusion and hypoxia

In all of our studies, following euthanasia, tumors were excised, fixed, embedded, and cut into cryosections for fluorescent imaging. To detect blood vessel perfusion, 75 μL of 0.6 mg/mL DiI dye (Invitrogen), dissolved in 75% dimethyl sulfoxide and then formulated in distilled deionized water, was administered i.v. 5 minutes prior to sacrifice. For the quantitative assessment of tumor hypoxia, 60 mg/kg pimonidazole was administered i.p. to mice 2 hours prior to sacrifice (36, 37). Excised tumors were subsequently prepared as cryosections, probed with Hypoxyprobe-1 (an FITC-conjugated monoclonal antibody that detects protein adducts of pimonidazole hydrochloride), according to manufacturer's recommendations (Hypoxyprobe-1 kit; Chemicon International). Tumor sections were then imaged for fluorescent intensity and analyzed, as described below.

Image acquisition and analysis

Tumor sections were imaged using a fluorescence microscope (BD CARV II Confocal Imager; BD Biosciences), a Quentem 512sc Photometrics camera (Photometrics), and a

MIV2000 motorized x-y stage (MetaMorph Imaging System; Molecular Devices), at the following excitation/emission (Ex/Em) wavelengths: HA, DiI, and CD31: 562 nm/624 nm; Hypoxyprobe-1, ColI, and α-SMA: 490 nm/520 nm.

Captured Hypoxyprobe-1 and ColI images were then analyzed with Image-Pro Analyzer 7.0 software (Media Cybernetics). For α-SMA quantification, bright field slides were scanned using the Aperio AT2 scanner (Leica Biosystems), and images were analyzed with HALO image analysis software (Indica Lab). Necrotic regions were excluded from analysis. The percent fluorescent positive area was calculated as the fluorescent signal area divided by the entire tumor area (% positive area = positive signal area/total area). HA levels were quantified using the Spectrum Positive Pixel Count V9 Aperio scoring algorithm (Leica Biosystems).

Tumor doxorubicin distribution

Murine KLN205 and human xenograft H2170/HAS3 tumor–bearing mice were staged into three groups to be treated with vehicle, PEGPH20 at 0.0375 or 1 mg/kg, 3 hours prior to sacrifice (38). Tumors were harvested and embedded in optimum cutting temperature compound, frozen on dry ice, and stored at −80°C. Single cryostat sections (7 μm thick) were cut from each tumor, mounted on glass slides, and allowed to air-dry. Doxorubicin autofluorescence was detected using a microscanner (see above) at Ex/Em 490 nm/520 nm. Subsequent to imaging of doxorubicin, tissue sections were fixed and stained with rat anti-CD31 (1:100; Pharmingen) for 1 hour and then revealed by secondary Alexafluor 594 anti-rat IgG (Jackson ImmunoResearch) for 30 minutes. Sections were then washed and incubated with FITC-Hypoxyprobe-1 for 1 hour. Finally, sections were washed in PBS and air-dried for fluorescent imaging. Tissue sections were reimaged in an identical way to that used to capture doxorubicin fluorescence. Composite images of doxorubicin, CD31, and Hypoxyprobe-1 were generated using MetaMorph Imaging System (version 8.0; Molecular Devices). Regions of interest were selected from each tissue section. Doxorubicin intensity was averaged over all pixels at given distance to the nearest vessel and plotted as a function of distance to the nearest vessel.

Quantitative assessment of tumor vascular volume

Relative tumor vascular volume (blood volume) was determined using a Vevo 2100 micro-imaging system in nonlinear contrast mode, coupled with hyperechoic MicroMarker Contrast Agent microbubbles (MBs; FUJIFILM VisualSonics). The tumor vascular volume in mice bearing AsPC-1 or AsPC-1/HAS3 tumors was determined 1 hour after second dose of vehicle or PEGPH20 (0.0375 or 1 mg/kg, i.v.). Briefly, animals were anesthetized, a 3D image of the entire tumor was obtained (i.e., total tumor volume), and a bolus of MBs (50 μL at 2×10^9 MBs/mL) was injected (i.v.). MBs were given for 2 minutes for systemic distribution, and then a second 3D image was acquired. Images were analyzed using VevoCQ software (FUJIFILM VisualSonics), and vascular volume was presented either as absolute volume (mm^3) or as relative to normalized tumor volume of the vehicle control (defined as 1).

Tumor extracellular pH

AsPC-1/HAS3 tumor–bearing mice were staged to receive API buffer or PEGPH20 at 0.0375 mg/kg i.v. when tumors reached ~700 mm^3. AcidoCEST MRI extracellular pH (pHe) measurements were taken before and 24 and 72 hours after PEGPH20 treatment as previously described (39). In brief, tumor-bearing mice were anesthetized, a tail vein catheter inserted, and a bolus of 200 μL iopamidol was administered, followed by a continuous iopamidol infusion (150 μL/h). The acidoCEST MRI protocol was repeated for 5 scans at 4.8 minutes per scan, or a total scan time of ~25 minutes. The pHe was calculated based on a calibration performed using an identical acidoCEST MRI protocol, log ratio of the CEST amplitudes of iopromide. Contrast agent uptake was calculated as the number of pixels with pHe within the range of pH 6.2 to 7.0 and pixels with pH >7.0, relative to the total number of pixels that represent the tumor. Data were normalized relative to baseline vehicle control (defined as normalized pHe = 1), and changes in pHe expressed as percent normalized pHe ± SEM.

Correlation between ColI and HA in human pancreatic tumor sections

ColI and HA staining was assessed in 44 patient samples (IHC for HA and ColI at the same time point), and staining intensity scored from 0 to 3 (0, negative; 1, weak; 2, moderate; 3, strong; see ref. 2). The reported score for each patient was an average from two or more core samples (per patient). Independent assessments were made of percentage of stained area and staining intensity following review of multiple random images taken from digitally scanned slides. JMP (version 13.2.0; SAS Institute, Inc. 2017. JMP 13, Cary NC) was used to assess the correlation between ColI and HA, and a Pearson correlation coefficient was determined.

Tumor microdialysis sampling and analysis of HA and VEGF-A165-A in collected tumor dialysate

Mice bearing peritibial murine CT26/HAS3 tumors received control vehicle or PEGPH20 at 0.0375 or 1 mg/kg, i.v. 24 hours prior to microdialysis. Mice were anesthetized using isoflurane, and a heating pad was used to maintain body temperature. A small incision was made on the tumor. A microdialysis probe with 100,000 Da molecular weight cut-off (CMA) was inserted into the tumor, using a guided cannula. The length of the microdialysis probe used in this study was 10 mm. Once the probe was in position, the cannula was withdrawn leaving the probe completely embedded in the tumor tissue.

Dulbecco’s PBS with protease inhibitors was perfused through the probe at a flow rate of 1 μL/min for 30 minutes to collect samples. For VEGF-A165-A, tumor dialysates were analyzed using Milliplex Map kit (Mouse Cytokine/Chemokine Magnetic Bead Panel; EMD Millipore). In brief, 25-μL samples were added to pretreated 96-well plates and incubated overnight at 4°C. After the plates were washed, 25 μL of detection antibody was added and incubated for 1 hour at room temperature. Then, 25-μL streptavidin–phycoerythrin was added and incubated for 30 minutes at room temperature. Plates were washed, and 150 μL of sheath fluid was added; 5 minutes later, plates were read by Luminex 200 (EMD Millipore). To dialyze HA fragments, a microdialysis probe with a 55,000 Da molecular weight cut-off (CMA) was placed into AsPC-1/HAS3 or H2170/HAS3 tumors using a guided cannula. Tumor dialysate samples were collected prior to, and at 1, 2, 3, 6, and 24 hours following

PEGPH20 administration (0.0375 mg/kg, i.v.). Microdialysis perfusates were analyzed using an enzyme-linked HA-binding protein sandwich assay (Cat# DY3614; R&D Systems) according to manufacturer's instructions as previously described (27).

Statistical analysis

One-way ANOVA or Student *t* test was applied to all of our studies to compare the mean value among groups or between parental and HAS3 groups, or between vehicle control and PEGPH20-treated groups. The level of significance was defined as $P < 0.05$. Percentage change was calculated by the following formula: (Mean of control group – Mean of treated group)/Mean of control group × 100%.

Results

Accumulation of HA in tumors is correlated with hypoxia

We and others have shown in multiple tumor models, including traditional cell-derived xenografts, patient-derived xenografts, and genetically engineered mouse models, that tumor accumulation of HA is associated with increased tIP and the collapse of tumor vasculature (1, 8, 9). Based upon these findings, we speculated that accumulation of HA in tumors would correlate with increasing hypoxia, which would be modulated toward normoxia following *in vivo* enzymatic reduction of tumor HA with PEGPH20. We evaluated tumor HA content, relative tumor perfusion, hypoxia, change in apparent extracellular pH, and doxorubicin penetration, which reflects blood vessel patency and overall tumor perfusion, in both immune competent and immunodeficient mouse models (Fig. 1).

In order to modulate the amount of HA in each tumor, we used two methods. The first method was to prepare lentivirus-mediated HA synthase-overexpressing tumor cells, which could be compared with the parental cell line for properties *in vivo* (40). The second method was to treat tumor-bearing mice with vehicle, a low dose of PEGPH20 (0.0375 mg/kg), equivalent to a human dose (3 μg/kg, determined by allometric scaling) being evaluated in clinical trials (e.g.,), or a high dose of PEGPH20 (1 mg/kg), a dose which is known to deplete most tumor HA in mouse models (27). These treatments resulted in tumors with varying amounts of HA (Fig. 1A, insets). Tumors from mice that had been treated with each of the PEGPH20 dose levels (vehicle, 0.0375 and 1 mg/kg) were then harvested, fixed, and later sectioned for histologic analysis.

The HA-accumulating murine KLN205 lung cancer control tumors (Fig. 1A, left plot) show highly compressed blood vessels (staining with anti-CD31 antibody; red color). After treatment with i.v. doxorubicin, extravasation was limited in the HA-accumulating microenvironment (Fig. 1A, left plot; blue color). As expected, IHC assays showed that vascular collapse and diminished doxorubicin staining cooccurred with hypoxia in untreated mice (detected by Hypoxyprobe-1; Fig. 1A; green color). The partial removal of HA with low-dose PEGPH20 (0.0375 mg/kg; Fig. 1A, center plot) resulted in a visible expansion of blood vessels, decreased hypoxia, and a clear increase in doxorubicin penetration relative to vehicle-treated mice (Fig. 1A, left vs. center plot). Treatment with high-dose PEGPH20 (1 mg/kg), which resulted in essentially complete HA removal, was associated with a further

decrease in tumor hypoxia, and a further increase of doxorubicin extravasation (Fig. 1A, right plot). Direct measure of the area of doxorubicin "halos" around blood vessels (Fig. 1B) showed that doxorubicin penetration into the tumor was increased by 44.6% at the 0.0375 mg/kg dose, and an additional 17% increase (total ~68% increase) at the 1-mg/kg dose (MuKLN205, Fig. 1B, left plot). In experiments using the human lung squamous cell carcinoma (SCC) model (H2170/HAS3), derived from the human SCC H2170 cell line engineered to overexpress HAS3, and shown to accumulate HA *in vivo* (Fig. 1 and unpublished data), similar results were obtained; namely, that HA removal correlated with increased doxorubicin penetration and dispersion (Fig. 1B, right plot). Additional studies in human AsPC-1/HAS3 or H2170/HAS3 tumor-bearing mice, using microdialysis to evaluate the time course of the disappearance of HA within the tumor extracellular milieu following low-dose PEGPH20 treatment (0.0375 mg/kg), have resulted in an eightfold or 15- to 20-fold increase in free intratumoral HA (depending upon the model used) at 2 to 4 hours after dosing (Fig. 1C), which is consistent with the rapid changes observed in tumor-associated HA and increased perfusion of doxorubicin. The subsequent fall in extracellular tumor HA at later time points may be attributed to movement of HA fragments into the lymph and circulation for hepatic and/or renal clearance (41, 42). A third model of the differential impact of reducing HA in tumors was performed using the pancreatic cancer cell line AsPC-1-P (parental) xenografts compared with AsPC-1/HAS3 (HA-accumulating) xenografts before and after treatment with PEGPH20 (Fig. 2A). Significant differences in tumor perfusion were observed only in the HA-high ASPC-1/HAS3 model (Fig. 2A, left plot). The AsPC-1/HAS3 tumors also demonstrated increased total (3D) vascular volume (Fig. 2A, middle plot) and decreased hypoxic area (Fig. 2A, right plot) following *in vivo* exposure to PEGPH20. The robust changes observed in all three physical parameters (increased perfusion, increased vascular volume, and decreased hypoxia) in the HA-accumulating AsPC-1/HAS3 tumors were not surprising, in that HA levels were reduced by >64% following low-dose PEGPH20 administration (Supplementary Fig. S1).

A summary of experiments comparing six different tumor xenografts with known HA content is shown in Fig. 2C (and Supplementary Fig. S2). In each case, the HA-accumulating tumors demonstrate dramatic changes in tumor vascular volume and hypoxia following high-dose PEGPH20. When tumor-associated hypoxia-inducible factor 1-alpha (HIF-1α) was evaluated in the H2170/HAS3 xenografts, the high dose of PEGPH20 (1 mg/kg) was associated with a 78% reduction in HIF-1α tumor expression (Supplementary Fig. S3). In a separate study in AsPC-1/HAS3 tumor–bearing mice, we investigated how increased perfusion/vascular volume and decreased hypoxia would affect tumor pHe. As expected, these physiologic changes were accompanied by a small but significant increase in apparent intratumoral pHe (Fig. 2B).

Tumor content of collagen and α-SMA increase coordinately with increased HA content in tumors

Collagen and HA are important components of most solid tumors, and their accumulation is often associated with a worsened prognosis (2). Because they have overlapping functions in the TME, e.g., increased tIP and tumor "stiffness" (8, 9, 43), we aimed to determine whether ectopic expression of HAS3, with associated increased accumulation of HA *in vivo* (40),

would affect the tumor in such a way that other indicators of tumor aggressiveness, in addition to the HA-high phenotype, would become evident. For this purpose, we examined the accumulation of collagen and α-SMA, which has similarly been found to predict a more rapid course of disease in pancreatic cancer patients (44). Overexpression of HAS3 led to a parallel accumulation of HA, collagen, and increased α-SMA expression in both the AsPC-1/HAS3 and BxPC-3/HAS3 pancreatic tumor xenografts in nude mice (Fig. 3A–C). These results are consistent with the hypothesis that collagen and HA cooperate in building the stromal compartment of the tumor.

We then investigated the correlation between accumulation of ColI and HA in samples from a study in human pancreatic cancer patients. The patient population and the independent correlation of either ColI or HA accumulation with more aggressive pancreatic cancer have been described (2). Data from this study were recompiled, and the Pearson correlation coefficient was determined to be 0.902 (R^2 = 0.813), suggesting a correlation between ColI and HA accumulation in tumors, further supporting the hypothesis that collagen and HA cooperate in the building of the tumor stroma (Fig. 3D). Although this observation is based on a limited number of patients (see Methods; ref. 2), it is consistent with our results in both syngeneic and xenograft mouse tumor models. This observation suggests that tumor cells which ectopically express HA synthase and consequently accumulate more collagen should grow more aggressively than tumors low in HA. This concept is supported by experiments in the faster-growing AsPC-1/HAS3 tumors that demonstrated a 3.5-fold accumulation of stromal HA as compared with the parental AsPC-1 tumors (AsPC-1-P; Supplementary Fig. S4; ref. 39). These results are supported by similar data that have been previously reported (40, 45). Thus, the HA-associated coaccumulation of collagen and increased α-SMA may reflect the creation of a more robust stroma for tumor growth (9).

Remodeling of the TME mediated by enzymatic removal of tumor HA

The amount of HA accumulation in tumor xenografts predicts tumor responsiveness to treatment with PEGPH20 in animal models (8, 27) and in pancreatic cancer patients (46). In the present study, as well as in previous work (3, 8, 9), the HA-accumulating TME also contains numerous proteoglycans, many of which are decorated with glycosaminoglycans like heparan sulfate, which bind many growth factors and cytokines (47), and chondroitin sulfate, which binds VEGF-A165 (48). PH20 hyaluronidase (precursor to PEGPH20) is known to use HA and the chemically closely related chondroitin sulfates as substrates, but not other glycosaminoglycans (49). Because of our findings that HA-accumulating tumors are hypoxic and contain chondroitin sulfate in addition to HA, and the pegylated version also degrades chondroitin sulfate (data not shown), we suspected that PEGPH20 treatment would also degrade the chondroitin sulfate component of the matrix, leading to tumor depletion of VEGF-A165.

Accordingly, to determine if VEGF-A165 was depleted from the HA-accumulating TME following enzymatic degradation of HA via PEGPH20, we treated immune competent Balb/c mice bearing CT26/HAS3 tumors with PEGPH20, and evaluated the soluble VEGF-A165 levels at 24 hours after PEGPH20 treatment (Fig. 4). Treatment with PEGPH20 depleted measurable VEGF-A165 to an undetectable level, both at the human equivalent

dose of 0.0375 mg/kg and at 1 mg/kg. The measurable levels of another 28 assayed cytokines and growth factors were not significantly affected (data not shown; see methods for reference to analytes measured in the assay).

Discussion

The data described in this study suggest that HA accumulation plays a central role in remodeling the TME for tumor progression. As solid tumors progress, they accumulate collagen, proteoglycans, and glycosaminoglycans in the TME, and these glycomic and proteomic components function in a coordinated manner to create collapsed vasculature and hypoxia, predisposing cancers to metastasis (50). Growth factors, cytokines, and chemokines produced by malignant or nonmalignant cells within the tumor can bind to stromal components, thus creating a constantly improving environment for tumor progression (51–54).

Many tumors are characterized by stromal accumulation of HA, which causes increased tIP, vascular collapse, hypoxia, and inherent resistance to drug therapy. tIP, as it is used here, is a combination of solid stress and interstitial fluid pressure (55, 56). Through its coaccumulation with collagen, HA likely acts as a driver of tumorigenesis (57). The accumulation of HA is also associated with increased tumor-associated α-SMA, and a higher risk of metastasis, which is consistent with the observation that HA-high tumors have a worsened prognosis (53, 54, 58).

Accumulation of HA is associated with loss of plasma membrane E-cadherin and accumulation of cytoplasmic B-catenin, suggesting disruption of adherens junctions, shown in xenografts and in samples from patients treated with PEGPH20 (40). In further support of these concepts, we and others have shown that ectopic expression of HAS3 in xenografts increases their aggressiveness *in vivo* (Supplementary Fig. S4; refs. 40, 45). Significantly, results from a phase I trial showed that PEGPH20 led to release of soluble HA into the blood, increased tumor perfusion as measured by dynamic contrast enhanced MRI, and decreased uptake of ^{18}F-FDG in some patients (59). In addition, our results also show that PEGPH20-mediated reduction of tumor HA results in a decrease in the proangiogenic growth factor VEGF-A165. This underlies an important potential value of PEGPH20 as an anti-angiogenic therapy in HA-accumulating tumors. The release of VEGF-A165 is likely the result of PEGPH20-mediated chondroitinase activity and the tumor depletion of chondroitin, which is known to sequester VEGF-A165-A (46, 47). Exposure of HA-accumulating tumor xenografts to PEGPH20 also decreased the level of tumor-associated HIF-1α (Supplementary Fig. S3), which likely results in lower expression of VEGF-A165 (60). Coupled with chondroitinase-mediated VEGF-A165 depletion, and increased perfusion, it is likely that PEGPH20 has created a much less angiogenic TME. Our results are also consistent with an earlier observation that tumors resistant to antiangiogenic therapy become more sensitive after HA degradation with a pegylated PH20 (43).

Change in cytokines/chemokines following enzymatic HA reduction is the subject of ongoing work. Collagen has long been associated with hypoxia (10, 61) and highly desmoplasmic tumors, such as pancreatic cancer. It is thought to be a critical component of

the TME. It binds to multiple receptors with diverse biological consequences, including integrins, which contribute to stabilization of the extracellular matrix and cell adhesion (62). The coaccumulation of collagen and HA in nude mouse xenografts, syngeneic tumors, and patient samples indicates that the two have a basic and complementary function in tumorigenesis. The results reported here are also consistent with our earlier report that PEGPH20-mediated HA reduction in tumors is associated with a decrease in collagen synthesis *in vivo* (27), which further links the two molecules as codependent components of the TME. We have also shown in earlier work (27) that the reduction of HA in HA-accumulating tumors leads to reduced expression of ColI-a1, Col5 alpha, and tenascin C, suggesting that the enzymatic reduction of HA in HA-accumulating tumors results in extensive TME remodeling. In addition, earlier experiments have shown that HA-accumulating tumors lose plasma membrane E-cadherin and display accumulation of cytoplasmic B-catenin, suggesting disruption of adherens junctions (40). The decreased expression of tenascin C reported earlier (27) is also of interest because tenascin C has been implicated in stromal inflammation in tumor progression, and its depletion would be expected to result in decreased stromal inflammation (63, 64). Furthermore, phase II clinical data have shown that patients treated with gemcitabine/abraxane have an improved progression-free survival if PEGPH20 is added to the regimen (65). Other investigators, using independent means of depleting HA from HA-accumulating tumors, have reached similar conclusions to those described here (66, 67).

These new results provide further proof that enzymatic degradation of HA has a significant remodeling effect on HA-accumulating tumors by affecting many properties of the TME, and is likely to create an environment less compatible for tumor progression. In this article, we have shown that PEGPH20-mediated HA degradation in HA-accumulating tumors results in multiple connected therapeutic events, including vascular expansion, reduced hypoxia, increased extracellular pH, and depletion of tumor-associated VEGF-A165. Further work will focus on how these changes may be associated with mechanical–structural changes in the TME, especially as they may lead to novel therapeutic approaches to HA-high malignancies.

Supplementary Material

Refer to Web version on PubMed Central for supplementary material.

Acknowledgments

We thank Rebecca Symons for assistance with histology and Scott Patton for assistance with article preparation. This study was supported by R01 (CA169281) grant (H. Han and D.D. Von Hoff) and a R21 (CA191923) grant (H. Han) from the NIH/NCI, and a grant from the National Foundation for Cancer Research (D.D. Von Hoff).

The costs of publication of this article were defrayed in part by the payment of page charges. This article must therefore be hereby marked *advertisement* in accordance with 18 U.S.C. Section 1734 solely to indicate this fact.

References

1. Jacobetz MA, Chan DS, Neesse A, Bapiro TE, Cook N, Frese KK, et al. Hyaluronan impairs vascular function and drug delivery in a mouse model of pancreatic cancer. Gut 2013;62:112–20. [PubMed: 22466618]

2. Whatcott CJ, Diep CH, Jiang P, Watanabe A, LoBello J, Sima C, et al. Desmoplasia in primary tumors and metastatic lesions of pancreatic cancer. Clin Cancer Res 2015;21:3561–8. [PubMed: 25695692]
3. Shepard HM. Breaching the castle walls: hyaluronan depletion as a therapeutic approach to cancer therapy. Front Oncol 2015;5:192. [PubMed: 26380222]
4. Multhaupt HA, Leitinger B, Gullberg D, Couchman JR. Extracellular matrix component signaling in cancer. Adv Drug Deliv Rev 2016;97:28–40. [PubMed: 26519775]
5. Karsdal MA, Manon-Jensen T, Genovese F, Kristensen JH, Nielsen MJ, Sand JM, et al. Novel insights into the function and dynamics of extracellular matrix in liver fibrosis. Am J Physiol Gastrointest Liver Physiol 2015;308:G807–830. [PubMed: 25767261]
6. Proteoglycans Halper J. and diseases of soft tissues. Adv Exp Med Biol 2014;802:49–58. [PubMed: 24443020]
7. Stylianopoulos T, Munn LL, Jain RK. Reengineering the physical micro-environment of tumors to improve drug delivery and efficacy: from mathematical modeling to bench to bedside. Trends Cancer 2018;4:292–319. [PubMed: 29606314]
8. Thompson CB, Shepard HM, O'Connor PM, Kadhim S, Jiang P, Osgood RJ, et al. Enzymatic depletion of tumor hyaluronan induces anti-tumor responses in preclinical animal models. Mol Cancer Ther 2010;9:3052–64. [PubMed: 20978165]
9. Provenzano PP, Cuevas C, Chang AE, Goel VK, Von Hoff DD, Hingorani SR. Enzymatic targeting of the stroma ablates physical barriers to treatment of pancreatic ductal adenocarcinoma. Cancer Cell 2012;21:418–29. [PubMed: 22439937]
10. Chauhan VP, Martin JD, Liu H, Lacorre DA, Jain SR, Kozin SV, et al. Angiotensin inhibition enhances drug delivery and potentiates chemotherapy by decompressing tumour blood vessels. Nat Commun 2013;4:2516. [PubMed: 24084631]
11. Jain RK, Martin JD, Stylianopoulos T. The role of mechanical forces in tumor growth and therapy. Annu Rev Biomed Eng 2014;16:321–46. [PubMed: 25014786]
12. Fang M, Yuan J, Peng C, Li YCollagen as a double-edged sword in tumor progression. Tumour Biol 2014;35:2871–82. [PubMed: 24338768]
13. Hockel M, Schlenger K, Aral B, Mitze M, Schaffer U, Vaupel P. Association between tumor hypoxia and malignant progression in advanced cancer of the uterine cervix. Cancer Res 1996;56:4509–15. [PubMed: 8813149]
14. Lopci E, Grassi I, Rubello D, Colletti PM, Cambioli S, Gamboni A, et al. Prognostic evaluation of disease outcome in solid tumors investigated with 64Cu-ATSM PET/CT. Clin Nucl Med 2016;41:e87–92. [PubMed: 26447388]
15. Juhasz A, Markel S, Gaur S, Liu H, Lu J, Jiang G, et al. NADPH oxidase 1 supports proliferation of colon cancer cells by modulating reactive oxygen species-dependent signal transduction. J Biol Chem 2017;292:7866–87. [PubMed: 28330872]
16. Mujcic H, Hill RP, Koritzinsky M, Wouters BG. Hypoxia signaling and the metastatic phenotype. Curr Mol Med 2014;14:565–79. [PubMed: 24894165]
17. Span PN, Bussink J. Biology of hypoxia. Semin Nucl Med 2015;45:101–9. [PubMed: 25704383]
18. Wilson WR, Hay MP. Targeting hypoxia in cancer therapy. Nat Rev Cancer 2011;11:393–410. [PubMed: 21606941]
19. Olive KP, Jacobetz MA, Davidson CJ, Gopinathan A, McIntyre D, Honess D, et al. Inhibition of Hedgehog signaling enhances delivery of chemotherapy in a mouse model of pancreatic cancer. Science 2009;324:1457–61. [PubMed: 19460966]
20. Diop-Frimpong B, Chauhan VP, Krane S, Boucher Y, Jain RK. Losartan inhibits collagen I synthesis and improves the distribution and efficacy of nanotherapeutics in tumors. Proc Natl Acad Sci U S A 2011;108:2909–14. [PubMed: 21282607]
21. Sherman MH, Yu RT, Engle DD, Ding N, Atkins AR, Tiriac H, et al. Vitamin D receptor-mediated stromal reprogramming suppresses pancreatitis and enhances pancreatic cancer therapy. Cell 2014;80–93. [PubMed: 25259922]
22. Papageorgis P, Polydorou C, Mpekris F, Voutouri C, Agathokleous E, Kapnissi-Christodoulou CP, et al. Tranilast-induced stress alleviation in solid tumors improves the efficacy of chemo- and nanotherapeutics in a size-independent manner. Sci Rep 2017;7:46140. [PubMed: 28393881]

23. Polydorou C, Mpekris F, Papageorgis P, Voutouri C, StylianopoulosT. Pirfenidone normalizes the tumor microenvironment to improve chemotherapy. Oncotarget 2017;8:24506–17. [PubMed: 28445938]
24. Voutouri C, Polydorou C, Papageorgis P, Gkretsi V, Stylianopoulos T. Hyaluronan-derived swelling of solid tumors, the contribution of collagen and cancer cells, and implications for cancer therapy. Neoplasia 2016;18:732–41. [PubMed: 27886639]
25. Sironen RK, Tammi M, Tammi R, Auvinen PK, Anttila M, Kosma VM. Hyaluronan in human malignancies. Exp Cell Res 2011;317:383–91. [PubMed: 21134368]
26. Zhou H, Fan Z, Deng J, Lemons PK, Arhontoulis DC, Bowne WB, et al. Hyaluronidase embedded in nanocarrier PEG shell for enhanced tumor penetration and highly efficient antitumor efficacy. Nano Lett 2016;16:3268–77. [PubMed: 27057591]
27. Jiang P, Li X, Thompson CB, Huang Z, Araiza F, Osgood R, et al. Effective targeting of the tumor microenvironment for cancer therapy. Anticancer Res 2012;32:1203–12. [PubMed: 22493350]
28. Brekken C, de Lange Davies C. Hyaluronidase reduces the interstitial fluid pressure in solid tumours in a non-linear concentration-dependent manner. Cancer Lett 1998;131:65–70. [PubMed: 9839621]
29. Brekken C, Hjelstuen MH, Bruland ØS, de Lange Davies C. Hyaluronidase-induced periodic modulation of the interstitial fluid pressure increases selective antibody uptake in human osteosarcoma xenografts. Anticancer Res 2000;20:3513–9. [PubMed: 11131655]
30. Malvicini M, Fiore E, Ghiaccio V, Piccioni F, Rizzo M, Olmedo Bonadeo L, et al. Tumor microenvironment remodeling by 4-methylumbelliferone boosts the antitumor effect of combined immunotherapy in murine colorectal carcinoma. Mol Ther 2015;23:1444–55. [PubMed: 26105158]
31. Nagy N, Kuipers HF, Frymoyer AR, Ishak HD, Bollyky JB, Wight TN, et al. 4-methylumbelliferone treatment and hyaluronan inhibition as a therapeutic strategy in inflammation, autoimmunity, and cancer. Front Immunol 2015;6:123. [PubMed: 25852691]
32. Damodarasamy M, Johnson RS, Bentov I, MacCoss MJ, Vernon RB, Reed MJ. Hyaluronan enhances wound repair and increases collagen III in aged dermal wounds. Wound Repair Regen 2014;22:521–6. [PubMed: 25041621]
33. Kaneko T, LePage GA. Growth characteristics and drug responses of a murine lung carcinoma in vitro and in vivo. Cancer Res 1978;38:2084–90. [PubMed: 418873]
34. Kultti A, Li X, Jiang P, Thompson CB, Frost GI, Shepard HM. Therapeutic targeting of hyaluronan in the tumor stroma. Cancers (Basel) 2012;4:873–903. [PubMed: 24213471]
35. Jadin L, Huang L, Wei G, Zhao Q, Gelb AB, Frost GI, et al. Characterization of a novel recombinant hyaluronan binding protein for tissue hyaluronan detection. J Histochem Cytochem 2014;62:672–83. [PubMed: 24891594]
36. Varia MA, Calkins-Adams DP, Rinker LH, Kennedy AS, Novotny DB, Fowler WC Jr, et al. Pimonidazole: a novel hypoxia marker for complementary study of tumor hypoxia and cell proliferation in cervical carcinoma. Gynecol Oncol 1998;71:270–7. [PubMed: 9826471]
37. Huxham LA, Kyle AH, Baker JH, Nykilchuk LK, Minchinton AI. Micro-regional effects of gemcitabine in HCT-116 xenografts. Cancer Res 2004;64:6537–41. [PubMed: 15374965]
38. Primeau AJ, Rendon A, Hedley D, Lilge L, Tannock IF. The distribution of the anticancer drug Doxorubicin in relation to blood vessels in solid tumors. Clin Cancer Res 2005;11:8782–8. [PubMed: 16361566]
39. Chen LQ, Howison CM, Jeffery JJ, Robey IF, Kuo PH, Pagel MD. Evaluations of extracellular pH within in vivo tumors using acidoCEST MRI. Magn Reson Med 2014;72:1408–17. [PubMed: 24281951]
40. Kultti A, Zhao C, Singha NC, Zimmerman S, Osgood RJ, Symons R, et al. Accumulation of extracellular hyaluronan by hyaluronan synthase 3 promotes tumor growth and modulates the pancreatic cancer microenvironment. Biomed Res Int 2014;2014:817613. [PubMed: 25147816]
41. Fraser JR, Engstrom-Laurent A, Nyberg A, Laurent TC. Removal of hyaluronic acid from the circulation in rheumatoid disease and primary biliary cirrhosis. J Lab Clin Med 1986;107:79–85. [PubMed: 3941296]

42. Jadin L, Bookbinder LH, Frost GI. A comprehensive model of hyaluronan turnover in the mouse. Matrix Biol 2012;31:81–9. [PubMed: 22142621]
43. Rahbari NN, Kedrin D, Incio J, Liu H, Ho WW, Nia HT, et al. Anti-VEGF-A165 therapy induces ECM remodeling and mechanical barriers to therapy in colorectal cancer liver metastases. Sci Transl Med 2016;8:360ra135.
44. Sinn M, Denkert C, Striefler JK, Pelzer U, Stieler JM, Bahra M, et al. α-Smooth muscle actin expression and desmoplastic stromal reaction in pancreatic cancer: results from the CONKO-001 study. Br J Cancer 2014;111;1917–23. [PubMed: 25314063]
45. Koyama H, Hibi T, Isogai Z, Yoneda M, Fujimori M, Amano J, et al. Hyperproduction of hyaluronan in neu-induced mammary tumor accelerates angiogenesis through stromal cell recruitment: possible involvement of versican/PG-M. Am J Pathol 2007;170:1086–99. [PubMed: 17322391]
46. Hingorani SR, Harris WP, Beck JT, Berdov BA, Wagner SA, Pshevlotsky EM, et al. Phase Ib study of PEGylated recombinant human hyaluronidase and gemcitabine in patients with advanced pancreatic cancer. Clin Cancer Res 2016;22:2848–54. [PubMed: 26813359]
47. Meneghetti MC, Hughes AJ, Rudd TR, Nader HB, Powell AK, Yates EA, et al. Heparan sulfate and heparin interactions with proteins. J R Soc Interface 2015;12:0589. [PubMed: 26289657]
48. Le Jan S, Hayashi M, Kasza Z, Eriksson I, Bishop JR, Weibrecht I, et al. Functional overlap between chondroitin and heparan sulfate proteoglycans during VEGF-A165-induced sprouting angiogenesis. Arterioscler Thromb Vasc Biol 2012;32:1255–63. [PubMed: 22345168]
49. Honda T, Kaneiwa T, Mizumoto S, Sugahara K, Yamada S. Hyaluronidases have strong hydrolytic activity toward chondroitin 4-sulfate comparable to that for hyaluronan. Biomolecules 2012;2:549–63. [PubMed: 24970149]
50. DiGiacomo JW, Gilkes DM. Tumor hypoxia as an enhancer of inflammation-mediated metastasis: emerging therapeutic strategies. Target Oncol 2018;13:157–73. [PubMed: 29423593]
51. Barbouri D, Afratis N, Gialeli C, Vynios DH, Theocharis AD, Karamanos NK. Syndecans as modulators and potential pharmacological targets in cancer progression. Front Oncol 2014;4:4. [PubMed: 24551591]
52. Koontongkaew S The tumor microenvironment contribution to development, growth, invasion and metastasis of head and neck squamous cell carcinomas. J Cancer 2013;4:66–83. [PubMed: 23386906]
53. Tlsty TD, Coussens LM. Tumor stroma and regulation of cancer development. Annu Rev Pathol 2006;1:119–50. [PubMed: 18039110]
54. Hanahan D, Coussens LM. Accessories to the crime: functions of cells recruited to the tumor microenvironment. Cancer Cell 2012;21:309–22. [PubMed: 22439926]
55. Chauhan VP, Boucher Y, Ferrone CR, Roberge S, Martin JD, Stylianopoulos T, et al. Compression of pancreatic tumor blood vessels by hyaluronan is caused by solid stress and not interstitial fluid pressure. Cancer Cell 2014;26:14–5. [PubMed: 25026209]
56. DelGiorno KE, Carlson MA, Osgood R, Provenzano PP, Brockenbough JS, Thompson CB, et al. Response to Chauhan et al.: interstitial pressure and vascular collapse in pancreas cancer-fluids and solids, measurement and meaning. Cancer Cell 2014;26:16–7. [PubMed: 25026210]
57. Albeiroti S, Soroosh A, de la Motte CA. Hyaluronan's role in fibrosis: a pathogenic factor or a passive player? Biomed Res Int 2015;2015:790203. [PubMed: 26583132]
58. Otranto M, Sarrazy V, Bonte F, Hinz B, Gabbiani G, Desmouliere A. The role of the myofibroblast in tumor stroma remodeling. Cell Adh Migr 2012;6:203–19. [PubMed: 22568985]
59. Infante JR, Korn RL, Rosen LS, LoRusso P, Dychter SS, Zhu J, et al. Phase 1 trials of PEGylated recombinant human hyaluronidase PH20 in patients with advanced solid tumours. Br J Cancer 2018;118:153–61. [PubMed: 28949957]
60. Unwith S, Zhao H, Hennah L, Ma D. The potential role of HIF on tumour progression and dissemination. Int J Cancer 2015;136:2491–503. [PubMed: 24729302]
61. Stylianopoulos T, Martin JD, Chauhan VP, Jain SR, Diop-Frimpong B, Bardeesy N, et al. Causes, consequences, and remedies for growth-induced solid stress in murine and human tumors. Proc Natl Acad Sci USA 2012; 109:15101–8. [PubMed: 22932871]

62. Leitinger B, Hohenester E. Mammalian collagen receptors. Matrix Biol 2007;26:146–55. [PubMed: 17141492]

63. Sun Z, Schwenzer A, Rupp T, Murdamoothoo D, Vegliante R, Lefebvre O, et al. Tenascin-C promotes tumor cell migration and metastasis through integrin α9b1-mediated YAP inhibition. Cancer Res 2018;78:950–61. [PubMed: 29259017]

64. Midwood KS, Chiquet M, Tucker RP, Orend G. Tenascin-C at a glance. J Cell Sci 2016;129:4321–7. [PubMed: 27875272]

65. Hingorani SR, Zheng L, Bullock AJ, Seery TE, Harris WP, Sigal DS, et al. HALO 202: randomized phase II study of PEGPH20 plus nab-paclitaxel/gemcitabine versus nab-paclitaxel/gemcitabine in patients with untreated, metastatic pancreatic ductal adenocarcinoma. J Clin Oncol 2018;36:359–66. [PubMed: 29232172]

66. Kultti A, Pasonen-Seppänen S, Jauhiainen M, Rilla KJ, Kärnä R, Pyöriä E, et al. 4-Methylumbelliferone inhibits hyaluronan synthesis by depletion of cellular UDP-glucuronic acid and downregulation of hyaluronan synthase 2 and 3. Exp Cell Res 2009;315:1914–23. [PubMed: 19285976]

67. Urakawa H, Nishida Y, Wasa J, Arai E, Zhuo L, Kimata K, et al. Inhibition of hyaluronan synthesis in breast cancer cells by 4-methylumbelliferone suppresses tumorigenicity in vitro and metastatic lesions of bone in vivo. Int J Cancer 2012;130:454–66. [PubMed: 21387290]

Translational Relevance

The tumor microenvironment consists of cellular and non-cellular components, such as hyaluronan (HA), other glycosaminoglycans, and proteoglycans. HA and collagen accumulation is associated with high tumor interstitial pressure, vascular collapse, and hypoxia in tumor cells. Here, we show that HA degradation using PEGylated PH20 hyaluronidase (PEGPH20) in HA-accumulating (HA-high) tumors is accompanied by a reversal of many properties associated with the HA-high phenotype in mouse xenograft models. We also show that the increased accumulation of collagen associated with HA-high tumors in mouse models is observed in patients with HA-high tumors, suggesting a coordinated modulation of HA and collagen content within these tumors. In addition, we demonstrate for the first time that PEGPH20-mediated HA degradation results in a decrease in VEGF-A165, likely mediated by the enzyme's chondroitinase activity. These results support the previously reported, multifaceted, antitumor activity of PEGPH20, and provide support for ongoing clinical trials of this agent.

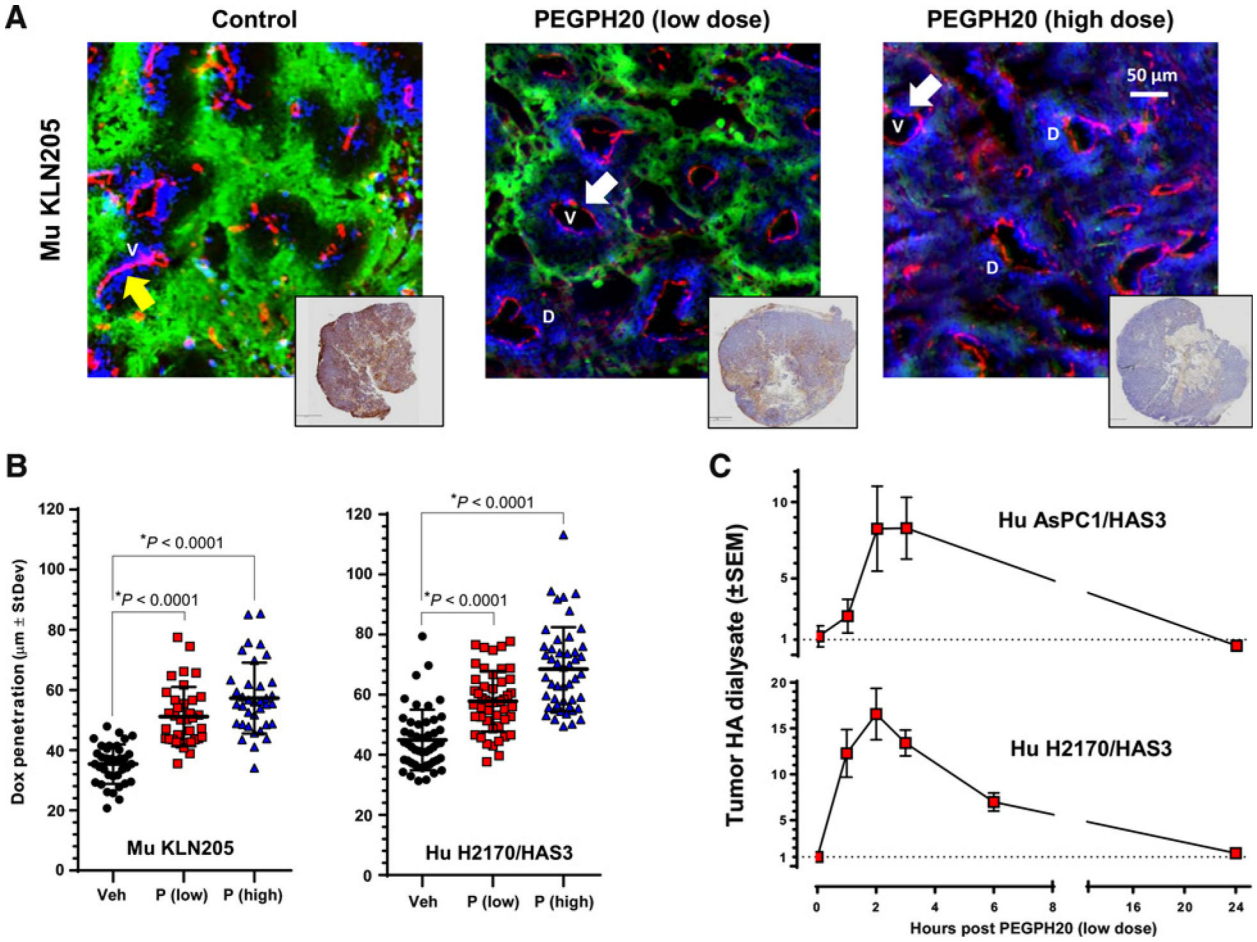

Figure 1.

Enzymatic degradation of tumor HA decreases tumor hypoxia, increases tumor doxorubicin penetration/dispersion, and increases free (nonbound, perfusable) HA within the tumor extracellular milieu. **A**, Representative images of murine SCC (KLN205) tumors treated i.v. with vehicle or PEGPH20, at 0.0375 mg/kg or 1 mg/kg, highlighting hypoxic regions (visualized with Hypoxyprobe-1, green), blood vessels (anti-CD31, red), and doxorubicin drug penetration (blue); with representative HA-stained (brown) whole tumor sections shown in accompanying insets. Arrows highlight closed (yellow) and open (white) tumor vessels. V, vessels and D, Doxorubicin. **B**, The area of doxorubicin penetration/dispersion increased in the murine KLN205 with low- (left plot) and high-dose (right plot) PEGPH20. **C**, Soluble HA fragments appear in the tumor dialysate (tumor interstitial fluid) immediately following PEGPH20 administration (0.0375 mg/kg, i.v.).

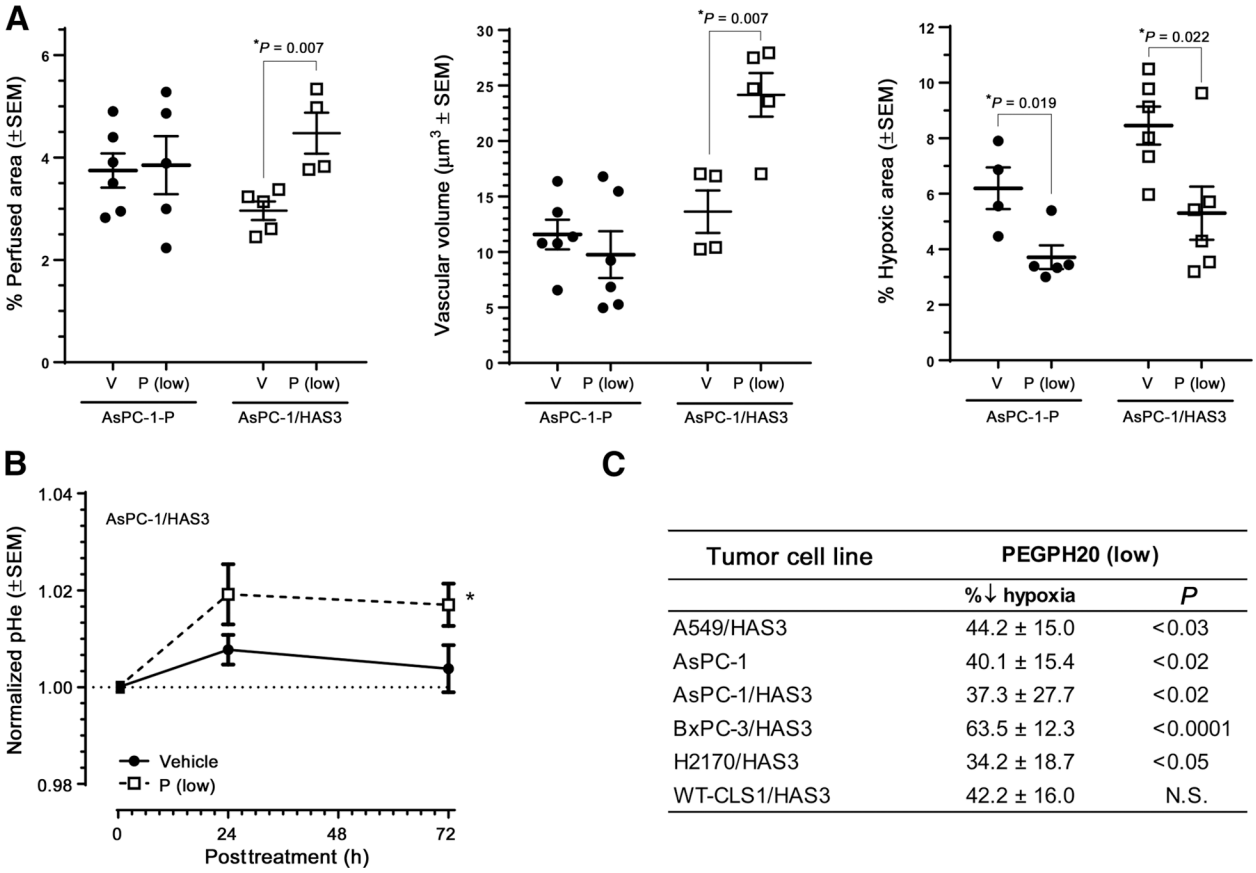

Tumor cell line	PEGPH20 (low)	
	%↓ hypoxia	*P*
A549/HAS3	44.2 ± 15.0	<0.03
AsPC-1	40.1 ± 15.4	<0.02
AsPC-1/HAS3	37.3 ± 27.7	<0.02
BxPC-3/HAS3	63.5 ± 12.3	<0.0001
H2170/HAS3	34.2 ± 18.7	<0.05
WT-CLS1/HAS3	42.2 ± 16.0	N.S.

Figure 2.

Enzymatic degradation of tumor HA increases tumor perfusion, vascular volume, and extracellular pH, while decreasing tumor hypoxia. **A**, Tumor HA degradation with low-dose PEGPH20 increased tumor perfusion (left plot), and vascular volume (middle plot), and reduced hypoxia (right plot) in HA-accumulating AsPC-1/HAS3. **B**, TME pHe increased after treatment with PEGPH20. **C**, A tabular list of six tumor xenografts and the relative decrease in hypoxia associated with low-dose PEGPH20 treatment.

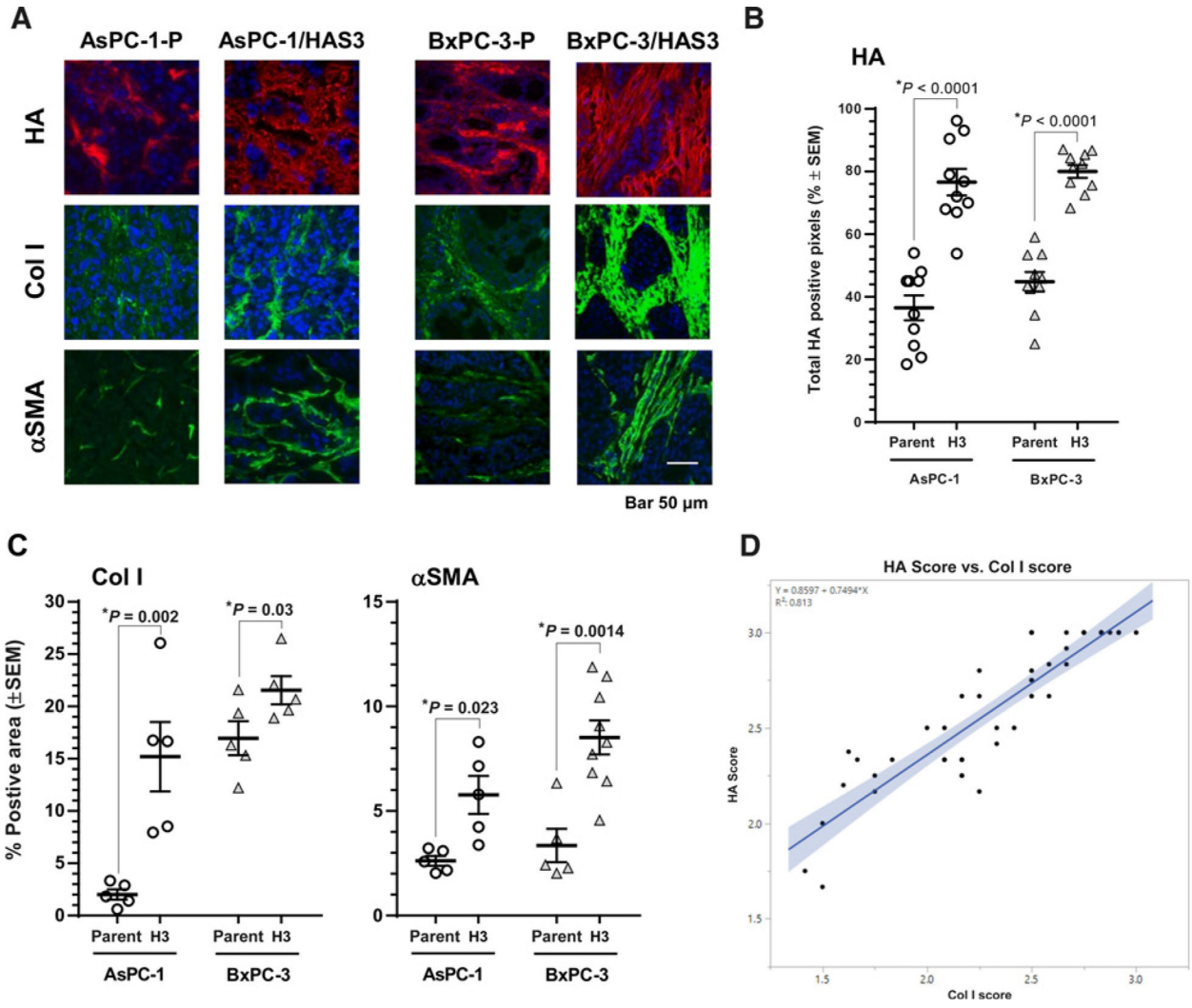

Figure 3.

HA accumulation is associated with increased collagen accumulation and α-SMA expression. **A**, Representative histology images of parental AsPC-1 (AsPC-1-P), AsPC-1/HAS3, parental BxPC-3 (BxPC-3-P), and BxPC-3/HAS3 xenograft tumors stained for HA (red), collagen I (green), and α-SMA (green). **B**, HAS3 transduction increased HA accumulation. **C**, HAS3 transduction increased the levels of tumor-associated ColI and α-SMA. **D**, In agreement with preclinical observations, there was a correlation (Pearson correlation coefficient = 0.902, R^2 = 0.813, confidence band α = 0.05) between ColI and HA in patient pancreatic tumor tissue sections.

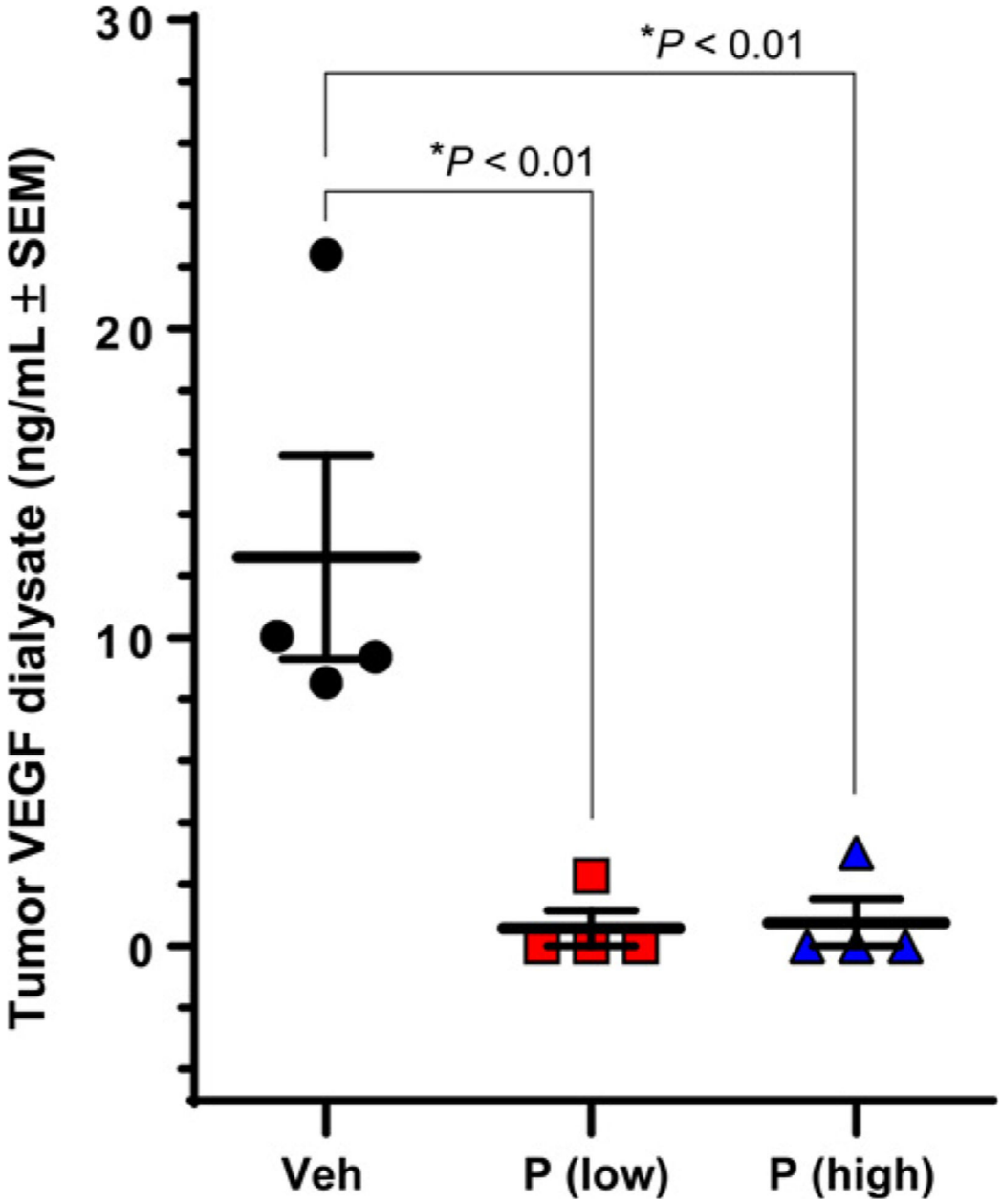

Figure 4.
Murine colorectal CT26/HAS3 extracellular VEGF-A165 at 24 hours after low-dose (0.0375 mg/kg) and high-dose (1 mg/kg) PEGPH20.